

Photocatalytic magnetic microgyroscopes with activity-tunable precessional dynamics

Dolachai Boniface,¹ Arthur V. Straube,^{2,3} and Pietro Tierno^{1,4,5,*}

¹*Departament de Física de la Matèria Condensada, Universitat de Barcelona, 08028 Spain*

²*Zuse Institute Berlin, TakustraÙe 7, 14195 Berlin, Germany*

³*Freie Universitat Berlin, Department of Mathematics and Computer Science, Arnimallee 6, 14195 Berlin, Germany*

⁴*Universitat de Barcelona Institute of Complex Systems (UBICS), Universitat de Barcelona, Barcelona, Spain*

⁵*Institut de Nanociencia i Nanotecnologia, Universitat de Barcelona, Barcelona, Spain*

(Dated: July 18, 2024)

Magnetic nano/microrotors are passive elements that spin around an axis due to an external rotating field while remaining confined to a close plane. They have been used to date in different applications related to fluid mixing, drug delivery or biomedicine. Here we realize an active version of a magnetic microgyroscope which is simultaneously driven by a photo-activated catalytic reaction and a rotating magnetic field. We investigate the uplift dynamics of this colloidal spinner when it stands up and precesses around its long axis while self-propelling due to the light induced decomposition of hydrogen peroxide in water. By combining experiments with theory, we show that activity emerging from the cooperative action of phoretic and osmotic forces effectively increase the gravitational torque which counteracts the magnetic and viscous ones, and carefully measure its contribution.

Spinning tops are mechanical anisotropic objects able of defying gravity while spinning around their vertical axis on a tiny tip [1]. When actuated by a twisting force, the tops can raise at a vertical position and precess slowly around an axis until friction and dissipation inevitably terminate their motion. Spinning tops are also part of mechanical gyroscopes, important for navigational systems [2, 3] and used as precise inertial sensors [1]. Thus, the macroscopic precession of anisotropic systems has been a subject of extensive research to date.

Recent years have witnessed an increasing interest in investigating the spinning motion of driven micro/nanoscale particles, due to their direct application in disparate technological fields including microfluidics [4–6], microrheology [7, 8], sensor [9, 10] and biotechnology [11]. Experimental realizations of precessing magnetic stirrers at such scale include ferromagnetic nanorods [12] or magnetic Janus colloids [13, 14], and have been recently used to investigate the entropy-driven thermal re-orientation of a single element [14] or the collective self-assembly process [15]. However, all these cases involve passive particles in absence of self-propulsion, which prevent the rotating element from moving and stirring across the plane.

In this context, ferromagnetic nanorods have been used in the past as microrheological tools [16–21], or to create localized microvortices able to trap [22–24] and stir [25, 26] non-magnetic tracer particles. Introducing activity via self-propulsion may lead to rich dynamic states with additional functionality. For example, an active magnetic rotor will be able to translate, and does not need to stop its rotational motion within the dispersing medium. As a matter of fact, passive micro/nano stirrers

lack of translational motion, which could only be induced by changing the plane of rotation of the applied field, i.e. when it rotates perpendicular to the sample plane [23] such that these particles stop stirring and behave as surface rotors [27–29].

Here we realize an active magnetic microgyroscope that combines two key elements: on one hand, it functions as a passive microgyroscope that spins due to a rotating magnetic field, and on the other, it operates as an active system exhibiting self-propulsion induced by an independent photoactivated chemical reaction. By illuminating with blue light, we measure an increase in the threshold field required to uplift and demonstrate that activity which results from phoretic and osmotic forces, enhances the gravitational torque effect by also pushing the particles toward the close plane. These results align well with a theoretical model that captures the main physical mechanisms governing the uplift dynamics.

Our active microgyroscopes are made of ferromagnetic hematite particles with a peanut shape, as shown in the small inset in Figure 1(a). This particular shape results from the sol-gel process used to synthesize them [30]. The fabricated particles are characterized by two connected lobes with a long (short) axis equal to $a = 2.6 \mu\text{m}$ ($b = 1.2 \mu\text{m}$). As observed in a previous work [31], hematite colloids become active when subjected to blue light in a water solution of hydrogen peroxide (H_2O_2). Their surface exposed to blue light catalyzes the decomposition of H_2O_2 in water, following the reaction: $2\text{H}_2\text{O}_{2(l)} \rightarrow \text{O}_{2(g)} + 2\text{H}_2\text{O}_{(l)}$. This reaction creates a chemical concentration gradient around the particles, inducing a diffusiophoretic flow. Due to this flow, the hematite particle can attract passive colloids nearby [32] and display self-propulsion [33].

We disperse the particles in an aqueous basic solution containing 3.6% by vol. of H_2O_2 , which is en-

* ptierno@ub.edu

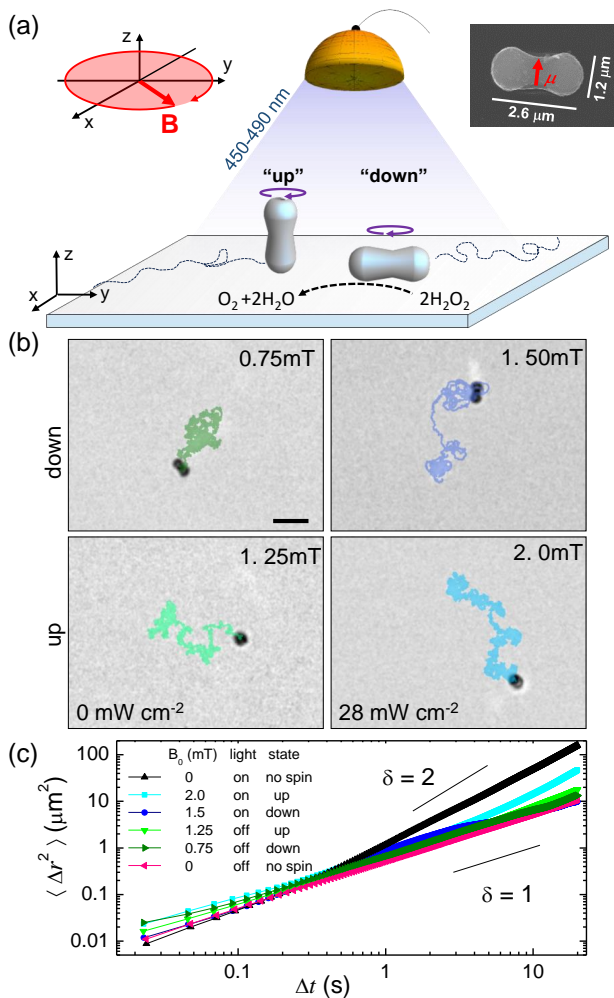


FIG. 1. (a) Schematic showing the two dynamic states, “up” and “down”, of a hematite particle under the combined action of a rotating magnetic field \mathbf{B} and the light induced decomposition of hydrogen peroxide (H_2O_2) in water. Small inset at the top right shows scanning electron microscope image of one hematite particle with the permanent moment μ superimposed. (b) Optical microscope images of the hematite particle in the down (top row) and up (bottom row) states in absence (first column) and in presence (second column) of blue light with the trajectories overlaid. The number at the top of each image shows the field amplitude of the rotating field, scale bar in the first image is $5 \mu\text{m}$. The corresponding video (Video S1) can be found in the Supporting Information. (c) Translational mean squared displacement $\langle \Delta r^2 \rangle$ versus lag-time Δt for spinning rotors in different dynamic states.

closed within a rectangular glass micro-tube (inner dimension $2 \times 0.1 \text{ mm}$). After a few minutes, the hematite particles sediment nearby to the bottom plate due to density mismatch, and display there diffusive dynamics. We induce self-propulsion by applying blue light at a wavelength $\lambda = 450 - 490 \text{ nm}$ with a tunable intensity $I \in [0, 125] \text{ mW cm}^{-2}$. Moreover, before the experiments, we employ an etching treatment with hydrochloric acid

to enhance the particle activity [33]. Additionally, we apply an external rotating magnetic field to induce spinning motion. This is possible since the hematite particles are slightly ferromagnetic, and display a small permanent dipole moment $\mu = 2 \times 10^{-16} \text{ A m}^2$ oriented along their short axis [34], Figure 1(a). More technical details on the experimental protocol and setup can be found in Section 1 of the Supporting Information.

We apply a rotating magnetic field circularly polarized in a plane (\hat{x}, \hat{y}) parallel to the glass substrate:

$$\mathbf{B} = B_0[\cos(\Omega t)\hat{x} - \sin(\Omega t)\hat{y}], \quad (1)$$

with B_0 the field amplitude, $\Omega = 2\pi f$, where f is the driving frequency. The hematite particles perform a spinning motion around their short axis with a frequency f_s , and for sufficiently low frequencies they rotate parallel to the bounding plane, which we refer to as the “down” state. In contrast, at intermediate frequencies, the particles preferentially stand up, performing a spinning motion around their long axis, thus perpendicular to the glass substrate, the “up” state, see Fig. 1(a). These two dynamic states can be controlled by adjusting B_0 and f , in addition to that we include the light activation, making these spinning rotors self-propelling. Fig. 1(b) displays typical trajectories of the hematite rotors in four possible situations: when they are in the down (top row) and up (bottom row) states and in presence of light (right column) or in absence of it (left column).

In absence of light, $I = 0$, the rotating hematite particles perform standard diffusive dynamics standing up or laying down, as shown by the measured translational mean squared displacement (MSD) in Fig. 1(c). Here we calculate the MSD as, $\langle \Delta \mathbf{r}^2(\Delta t) \rangle \equiv \langle (\mathbf{r}(t) - \mathbf{r}(t + \Delta t))^2 \rangle \sim \Delta t^\delta$, with $\mathbf{r}(t)$ the position of the particle center at time t , Δt the lag time and $\langle \dots \rangle$ a time average. The MSD can be used to distinguish between the normal diffusive ($\delta = 1$) dynamics from the sub-[super] diffusive ($\delta < 1$ [$\delta > 1$]) and ballistic ($\delta = 2$) ones. When the particles are activated by light ($I = 28 \text{ mW cm}^{-2}$) we find that in absence of spinning ($B_0 = 0$), the active particle exhibits a ballistic trajectory after few seconds with $\delta \sim 2$. In contrast, the spinning effect localizes the trajectories, reducing the corresponding exponent in the MSD. Specifically, we observe diffusive behavior for spinning down and super-diffusive, almost ballistic behavior for spinning up. This effect can be understood by observing that a rotating object in a viscous fluid generates an hydrodynamic flow field [35], which in first approximation is purely azimuthal and decays as $\sim 1/r^2$ [36]. Such flow may transport away the product of the catalytic reaction, reducing thus the concentration gradient around the particle and thereby the corresponding self-propulsion [37–39].

To gain insights in the different dynamic states, we have modified the model suggested in Ref. [12] to our situation, by incorporating the additional effect of the cat-

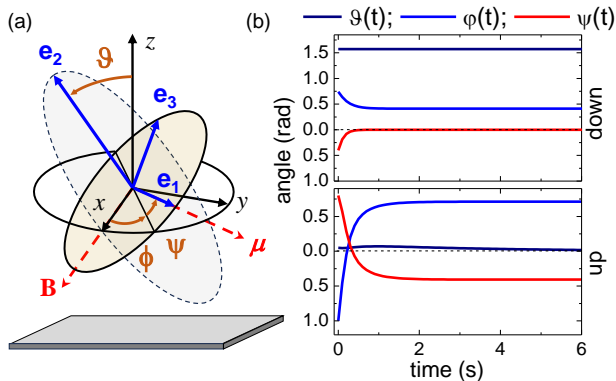


FIG. 2. (a) Schematic showing an elliptical particle (dashed line) with the laboratory reference frame $(\hat{x}, \hat{y}, \hat{z})$, the coordinate system fixed on the particle $(\hat{e}_1, \hat{e}_2, \hat{e}_3)$, the three Euler angles (ϑ, ϕ, ψ) , and the orientation of the applied magnetic field \mathbf{B} and magnetic moment $\boldsymbol{\mu}$. (b) Time evolution of the Euler angles from Eq. (3) for $\hat{B} = 5.0$ and at two different driving frequencies, $\hat{\Omega} = 2.0$ (down state, top panel, note $\vartheta = \pi/2$) and $\hat{\Omega} = 3.0$ (up state, bottom panel, note $\vartheta = 0$).

alytic reaction and the different geometry (shape). We approximate the particle as an ellipsoid with the major axis a and minor axis b , mass m , permanent moment $\boldsymbol{\mu}$ oriented along the minor axis and suspended in liquid medium of dynamic viscosity η . Further, as shown in Fig. 2(a), we have used two coordinate systems, the laboratory one $(\hat{x}, \hat{y}, \hat{z})$ and a second one that is fixed to the ellipsoid $(\hat{e}_1, \hat{e}_2, \hat{e}_3)$ with \hat{e}_1 and \hat{e}_3 aligned with $\boldsymbol{\mu}$ and the long axis of the ellipsoid, respectively. Both reference frames are connected through the Euler angles, (ϑ, ϕ, ψ) . In the absence of chemical activity, the overdamped motion of the ellipsoid is governed by the balance of different torques: magnetic, $\boldsymbol{\tau}_m = \boldsymbol{\mu} \times \mathbf{B}$, gravitational, $\boldsymbol{\tau}_g = ma(\hat{e}_3 \times \mathbf{g})/2$, and viscous, $\boldsymbol{\tau}_\eta = -\underline{\zeta} \boldsymbol{\omega}$, torques:

$$\underline{\zeta} \boldsymbol{\omega} = \boldsymbol{\mu} \times \mathbf{B} + \frac{1}{2}ma(\hat{e}_3 \times \mathbf{g}), \quad (2)$$

where \mathbf{g} is the gravitational acceleration, $\boldsymbol{\omega}$ is the angular velocity and $\underline{\zeta} = \text{diag}(\zeta_1, \zeta_2, \zeta_3)$, $\zeta_1 = \zeta_2 \neq \zeta_3$ is the rotational friction tensor in the main axes. Our main hypothesis is that the chemical activity generates an attractive phoretic/osmotic force $\mathbf{F}_{p/o}$ between the hematite and the substrate. This force gives rise to a corresponding torque, $\boldsymbol{\tau}_{p/o} = a(\hat{e}_3 \times \mathbf{F}_{p/o})/2$ which prevents the hematite from uplifting inducing an effective increase of the gravitational torque torque $\boldsymbol{\tau}_\downarrow = \boldsymbol{\tau}_{p/o} + \boldsymbol{\tau}_g$. Also, since the the hematite is pressed against the substrate there is a raise in the drag torque which now becomes $\boldsymbol{\tau}_d$. To take into account the effect of these osmotic/phoretic contributions avoiding the complex details of the corresponding chemical reactions, we introduce the dimensionless pref-

actor $\alpha \geq 1, \beta \geq 1$,

$$\boldsymbol{\tau}_\downarrow \rightarrow \alpha \boldsymbol{\tau}_g, \quad \boldsymbol{\tau}_d \rightarrow \beta \boldsymbol{\tau}_\eta$$

such that $\alpha = 1, \beta = 1$, for the system without activity.

Introducing dimensionless time, $\hat{t} = mga/(2\beta\zeta_1)t$, frequency, $\hat{\Omega} = 2\zeta_1\Omega/(mga)$, and field, $\hat{B} = 2\mu B_0/(mga)$, we arrive at the governing equations of motion:

$$\dot{\vartheta} = \left(\alpha + \hat{B} \sin \varphi \sin \psi \right) \sin \vartheta, \quad (3a)$$

$$\dot{\phi} = \beta \hat{\Omega} - \hat{B} \sin \varphi \cos \psi, \quad (3b)$$

$$\dot{\psi} = -\frac{\hat{B}}{1-\kappa} (\kappa \sin \varphi \cos \theta \cos \psi + \cos \varphi \sin \psi). \quad (3c)$$

Here, $\kappa = (\zeta_1 - \zeta_3)/\zeta_1$ specifies the particle's asymmetry and we have introduced the angle $\varphi = \phi - \Omega t$, implying the transition to the reference frame rotating together with the external field. The cases with $\vartheta = \pi/2$ and $\vartheta = 0$ describe the down and up states, respectively. For $\alpha = 1, \beta = 1$, Eq. (3) corresponds to the passive system [12], when the blue light and hence the activity are switched off. Figure 2(b) shows that Eq. (3) correctly predicts the two dynamic states experimentally observed by varying the field parameters. For a fixed value of the rescaled field, $\hat{B} = 5.0$ the stable state is the rod laying down ($\vartheta = \pi/2$) for low frequency, $\hat{\Omega} = 2.0$ (top panel), or standing up ($\vartheta = 0$) for large one, $\hat{\Omega} = 3.0$ (bottom panel).

We first characterize with experiments how the particle dynamics are influenced independently by the magnetic field (Fig. 3(a)) and by the activity (Fig. 3(b,c)). At low frequencies we observe the down state. Such state, where $\vartheta = \pi/2, \psi = 0$ is described by the single simplified equation, $\dot{\varphi} = \beta \hat{\Omega} - \hat{B} \sin \varphi$, cf. Eq. (3b). The latter equation predicts two dynamic regimes separated by a critical frequency f_c . Formulated in the dimensional units relative to the laboratory reference frame, for $f < f_c$ the particle rotates synchronously with \mathbf{B} , and its average spinning frequency $\langle f_s \rangle = f$, as shown by the black squares in Fig. 3(a). In contrast, for $f > f_c$ the particle still spins but does it in an asynchronous regime, where the average spinning drops down as, $\langle f_s \rangle = f[1 - \sqrt{1 - (f_c/f)^2}]$, see the disks in Fig. 3(a). These two regimes are connected by the critical frequency f_c which, as shown in the small inset in Fig. 3(a), scales linearly with the applied field as $f_c = \mu B_0/(2\pi\zeta_1)$. The data in such inset have been extrapolated from the non-linear regressions, since for a range of intermediate frequencies the spinning hematites were observed to enter in the up state rather than remained confined to the close plane. This effect is highlighted by the shaded green region in the graph in Fig. 3(a).

Our magnetic rotors can also be activated by blue light. In Fig. 3(b), we show the effect of the light induced decomposition of H_2O_2 , by measuring both the angular

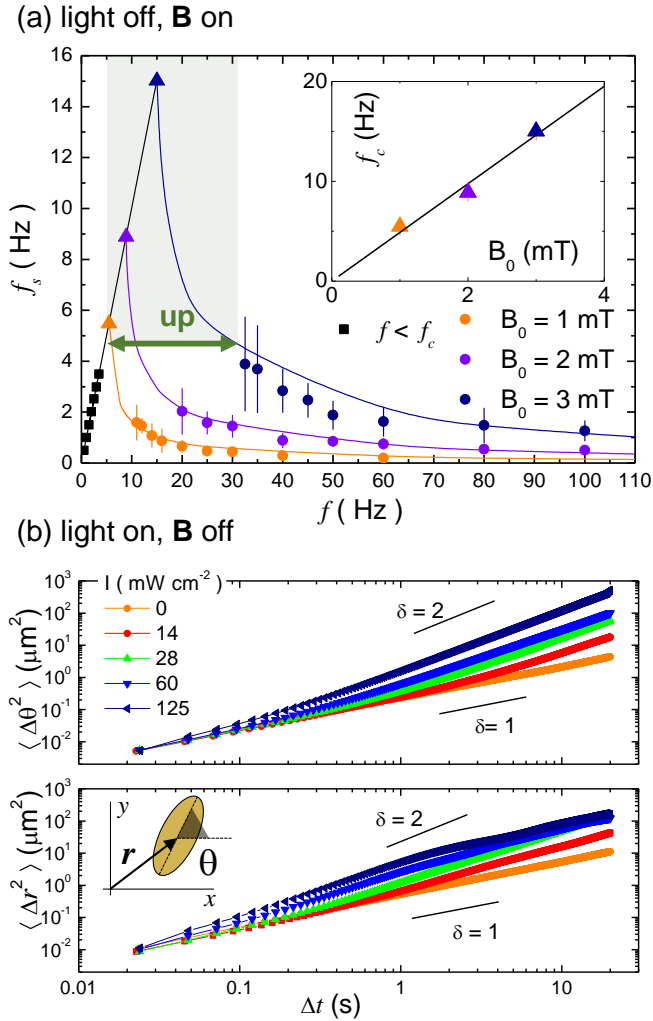


FIG. 3. (a) Spinning frequency f_s of a single hematite particle versus field frequency f for three field amplitudes B_0 . Scattered symbols are experimental data, continuous lines are non-linear regressions of the synchronous ($f < f_c$) and asynchronous ($f > f_c$) regimes. The triangles indicate the values of f_c extracted from these curves, and are shown in the top inset. The shaded green region in the graph indicates that the particle is in the up state. (b,c) Angular $\langle \Delta\theta^2 \rangle$ (b) and translation $\langle \Delta r^2 \rangle$ (c) mean squared displacements of a hematite particle in absence of magnetic field and under different light amplitudes I .

MSD $\langle \Delta\theta^2 \rangle$ (top) and the translational one, $\langle \Delta r^2 \rangle$ (bottom). In absence of light ($I = 0$), both MSDs show diffusive dynamics with a long-time rotational diffusion coefficient $D_\theta = 0.140 \pm 0.001 \text{ rad}^2 \text{ s}^{-1}$ and a translational one, $D_r = 0.152 \pm 0.001 \mu\text{m}^2 \text{ s}^{-1}$. However, when the light is on, the hematite particle becomes activated and displays a super-diffusive dynamics. This effect strongly emerges in the angular dynamics, where we initially observe a diffusive behavior followed by a superdiffusive/ballistic one at large Δt . The threshold between both dynamic

states decreases with the light amplitude I , and for the maximum power ($I = 125 \text{ mW cm}^{-2}$) it reduces to $\Delta t \sim 0.1 \text{ s}$. The effect of activity also changes the translational MSDs. Below a light intensity of $I \sim 50 \text{ mW cm}^{-2}$, we observed a diffusive behavior comparable to the case without activity, which then becomes superdiffusive beyond $\Delta t = 1 \text{ s}$. In contrast, for $I > 50 \text{ mW cm}^{-2}$ the behavior is first superdiffusive, then returns to diffusive for $\Delta t > 3 - 5 \text{ s}$. In this case we observe an enhanced diffusion with a coefficient which is more than 10 times higher than the passive case, $D_r \sim 2 \mu\text{m}^2 \text{ s}^{-1}$. This feature results from the etching process of the particles (see Method section), which roughens the particle surface enhancing the generated chemophoretic flow and the corresponding self-propulsion behavior.

We now consider the combined effect of the activity and spinning on the particle dynamics. The catalytic reaction induces self-propulsion due to a local gradient triggering osmotic and phoretic phenomena. Also, this reaction creates an effective attractive force between the hematite and the substrate. This force tends to elevate the threshold field \hat{B}_* required for the particle to transit towards the up state. We confirm this effect in Fig. 4(a), where we have measured \hat{B}_* by varying the light intensity, and thus the activity, in the (B_0, f) plane. Thus, the blue light shifts the limit \hat{B}_* towards higher magnetic amplitudes. From the model given by Eq. (3), it follows that the up and down state start to coexist at a critical field value,

$$\hat{B}_*(\hat{\Omega}) = \frac{1}{\alpha} \sqrt{(\alpha^2 + \beta^2 \hat{\Omega}^2)(\alpha^2 + \kappa^2 \beta^2 \hat{\Omega}^2)}. \quad (4)$$

The complete derivation of this equation is given in Section 2 of the Supplementary Material. Eq. 4 shows that, at low κ , changing α will shift the critical magnetic field amplitude, while changing β will alter the slope of the curve for sufficiently small Ω . In the latter case, we specifically verify this effect by increasing the viscosity of the solution through the addition of glycerol. In this specific scenario, we confirm that $\beta = \eta/\eta_w$, where η is the viscosity of the solution and η_w that of water, as shown in Section 3 of the Supplementary Information.

We use Eq. (4) to fit the experimental data describing the uplift transition induced by the rotational motion, Fig. 4(a). First we consider the transition in absence of activity, $I = 0$. Thus, we fix $\alpha = 1$, $\beta = 1$ and determine the remaining experimental parameter, here $\kappa = 0.0076$ and the rescaling prefactors. Next, we fix κ and change both α and β performing the simultaneous regression of all the experimental data obtained at different I . The multiple regression confirms the good agreement between the model and the experimental data. More importantly, this agreement highlights that the effect of activity effectively increases the vertical force pushing the particle towards the substrate. Even if the attraction is towards the nearby substrate, the presence of an

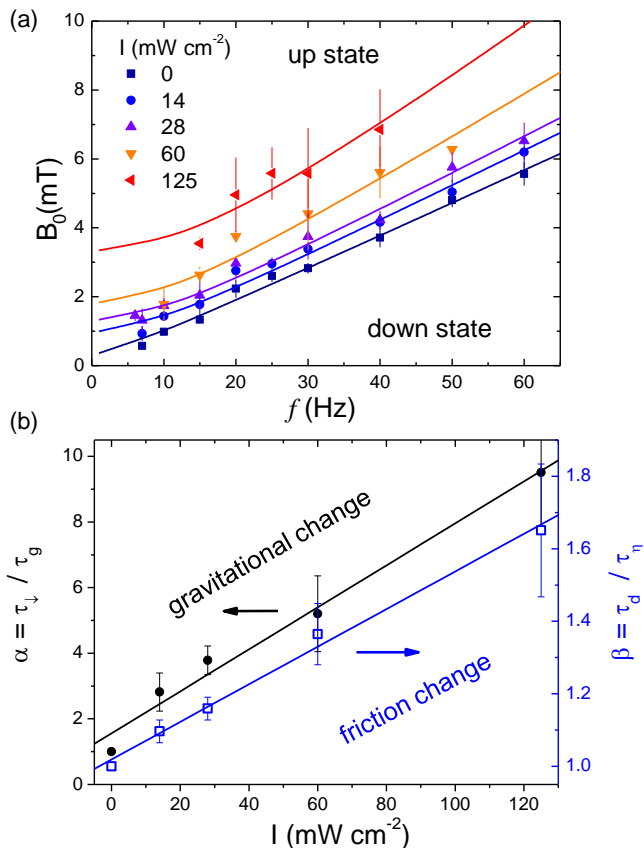


FIG. 4. (a) Border between the up and down states in the (f, B_0) plane and for different light intensities I . Scattered symbols are experimental data while continuous lines are non-linear regression from Eq. (4). (b) Evolution of the parameter α (black) indicating the raise of the gravitational-like torque (τ_g) due to the light intensity I , and β (blue) which corresponds to the variation of the friction torque (τ_{η}).

uplift force arising from the magnetic torque allows us to precisely measure this contribution. Indeed, from the variation of $\hat{B}_*(\hat{\Omega})$ it follows that α , which represent the intensity of attractive force relative to gravity, increases linearly with the light intensity. This phoretic/osmotic $\mathbf{F}_{p/o}$ force scales the gravity from up to 10 times for the maximum light intensity, $I = 125 \text{ mW cm}^{-2}$ and the light induced torque $\tau_{\downarrow} \propto \tau_g$, Fig. 4(b). Concerning the quantity β , which can be considered as a measure of the variation of the drag torque, it also increases with the light intensity but less drastically, as shown by the blue line in Fig. 4(b). This effect is due to the fact that the attractive phoretic force pushes the hematite close to the substrate, thus raising the hydrodynamic drag coefficients.

We finally comment on the origin of the chemically induced force $\mathbf{F}_{p/o} = \mathbf{F}_p + \mathbf{F}_o$, which results from both diffusiophoresis (\mathbf{F}_p) and diffusioosmosis (\mathbf{F}_o) contributions. The first one arises from a surface concentration gradient along the hematite surface, while the second

is due to a concentration gradient along the substrate. For both contributions, the surface concentration gradient $\nabla_{\parallel}\phi$, along the hematite or substrate, generates a slip velocity $u_{\text{slip}} \propto \nabla_{\parallel}\phi$, which leads to forces acting on the hematite [40] due to the generated hydrodynamic flow fields. Both components tend to push the particle toward the surface. The phoretic effect has been observed in previous works [31, 41] to induce an attraction between passive objects, as the substrate, and photocatalytic active hematite particles. For the osmotic component, the chemical activity of the hematite generates a radial concentration gradient along the substrate. The slip velocity over the substrate initiates a centripetal osmotic flow [40]. Due to the incompressibility of water, a vertical flow compensates for the radial flow, pushing the hematite against the substrate.

In conclusion, we have experimentally realized an active magnetic microgyroscope where spinning and activity are simultaneously and independently controlled by two different actuating fields. We investigate how spinning affects the microgyroscope transport and find that the rotational motion strongly suppresses self-propulsion compared to the zero magnetic field case. We then investigate the uplift dynamics when these gyroscopes are subjected to an in-plane rotating field and stand up to reduce viscous dissipation. In particular, by balancing all torques acting on the rotating particles, we find that the activity induced by a catalytic chemical reaction can be considered as an additional, gravitational-like torque, which increases the amplitude threshold field to transit the particle in the up state. We use a theoretical model to capture the basic physics of the process by balancing magnetism, gravity, viscosity and activity. These spinning self-propelling agents can be used in microfluidic channels as active component, adding further feasibility to previous experimental realizations based on passive (i.e. non-active) colloidal rotors [42, 43].

We thank Arkady Pikovsky for helpful discussions. This project has received funding from the European Research Council (ERC) under the European Union's Horizon 2020 research and innovation programme (grant agreement no. 811234). A. V. S. acknowledges support by the Deutsche Forschungsgemeinschaft (DFG) under Germany's Excellence Strategy–MATH+: The Berlin Mathematics Research Center (EXC-2046/1)–Project No. 390685689. P. T. acknowledges support from the Ministerio de Ciencia, Innovación y Universidades (grant no. PID2022- 137713NB-C21 AEI/FEDER-EU) and the Agència de Gestió d'Ajuts Universitaris i de Recerca (project 2021 SGR 00450) and the Generalitat de Catalunya (ICREA Acadèmia).

-
- [1] J. Perry, *Spinning Tops and Gyroscopic Motions* (reprinted by Dover, Sheldon, London, 1957).
- [2] K. Britting, *Inertial Navigation Systems Analysis* (John Wiley & Sons, Washington, DC, USA, 1971).
- [3] V. M. N. Passaro, A. Cuccovillo, L. Vaiani, M. D. Carlo, and C. E. Campanella, Gyroscope technology and applications: A review in the industrial perspective, *Sensors* **17**, 2284 (2017).
- [4] T. Sawetzki, S. Rahmouni, C. Bechinger, and D. W. M. Marr, In situ assembly of linked geometrically coupled microdevices, *Proc. Natl. Acad. Sci. U. S. A.* **105**, 20141 (2008).
- [5] B. Kavcic, D. Babic, N. Osterman, B. Podobnik, and I. Poberaj, Magnetically actuated microrotors with individual pumping speed and direction control, *Appl. Phys. Lett.* **95**, 023504 (2009).
- [6] W. H. Chong, L. K. Chin, R. L. S. Tan, H. Wang, A. Q. Liu, and H. Chen, Stirring in suspension: Nanometer-sized magnetic stir bars, *Angew. Chem. Int. Ed.* **52**, 8570 (2013).
- [7] J.-F. Berret, Local viscoelasticity of living cells measured by rotational magnetic spectroscopy, *Nature Comm.* **7**, 10134 (2016).
- [8] Y. Gu and K. G. Kornev, Ferromagnetic nanorods in applications to control of the in-plane anisotropy of composite films and for in situ characterization of the film rheology, *Adv. Func. Mater.* **26**, 3796 (2016).
- [9] J. P. Steimel, J. L. Aragonés, and A. Alexander-Katz, Artificial tribotactic microscopic walkers: Walking based on friction gradients, *Phys. Rev. Lett.* **113**, 178101 (2014).
- [10] K. Dhatt-Gauthier, D. L. Y. Wu, and K. J. M. Bishop, Accelerating the design of self-guided microrobots in time-varying magnetic fields, *JACS Au* **3**, 611 (2023).
- [11] X. Lyu, J. Chen, R. Zhu, J. Liu, L. Fu, J. L. Moran, and W. Wang, Active synthetic microrotors: Design strategies and applications, *ACS Nano* **17**, 11969 (2023).
- [12] P. Dhar, C. D. Swayne, T. M. Fischer, T. Kline, and A. Sen, Orientations of overdamped magnetic nanorod-gyroscopes, *Nano Lett.* **7**, 1010–1012 (2007).
- [13] J. Yan, M. Bloom, S. C. Bae, E. Luijten, and S. Granick, Linking synchronization to self-assembly using magnetic janus colloids, *Nature* **491**, 578 (2012).
- [14] Y. Gao, A. K. Balin, R. P. A. Dullens, J. M. Yeomans, and D. G. A. L. Aarts, Thermal analog of gimbal lock in a colloidal ferromagnetic janus rod, *Phys. Rev. Lett.* **115**, 248301 (2015).
- [15] J. Mecke, Y. Gao, C. A. R. Medina, D. G. A. L. Aarts, G. Gompper, and M. Ripoll, Simultaneous emergence of active turbulence and odd viscosity in a colloidal chiral active system, *Commun. Phys.* **6**, 324 (2023).
- [16] A. Anguelouch, R. L. Leheny, and D. H. Reich, Application of ferromagnetic nanowires to interfacial microrheology., *Appl. Phys. Lett.* **89**, 111914 (2006).
- [17] B. Frka-Petesic, K. Erglis, J. F. Berret, A. Cebers, V. Dupuis, J. Fresnais, O. Sandre, and R. Perzynski, Dynamics of paramagnetic nanostructured rods under rotating field, *J. Magn. Magn. Mat.* **323**, 1309 (2011).
- [18] A. Tokarev, I. Luzinov, J. R. Owens, and K. G. Kornev, Magnetic rotational spectroscopy with nanorods to probe time-dependent rheology of microdroplets, *Langmuir* **28**, 10064–10071 (2012).
- [19] L. Chevy, R. Colin, B. Abou, and J.-F. Berret, Intracellular microrheology probed by micron-sized wires, *Bio-materials* **34**, 6299 (2013).
- [20] A. Brasovs, J. Cimurs, K. Erglis, A. Zeltins, J.-F. Berret, and A. Cebers, Magnetic microrods as tool for microrheology, *Soft Matter* **11**, 2563 (2015).
- [21] M. Radiom, R. Hénault, S. Mani, A. G. Iankovski, X. Norel, and J.-F. Berret, Magnetic wire active microrheology of human respiratory mucus, *Soft Matter* **17**, 7585–7595 (2021).
- [22] L. O. Mair, B. Evans, A. R. Hall, J. Carpenter, A. Shields, K. Ford, M. Millard, and R. Superfine, Highly controllable near-surface swimming of magnetic janus nanorods: application to payload capture and manipulation, *J. Phys. D: Appl. Phys.* **44**, 125001 (2011).
- [23] T. Petit, L. Zhang, K. E. Peyer, B. E. Kratochvil, and B. J. Nelson, Selective trapping and manipulation of microscale objects using mobile microvortices, *Nano letters* **12**, 156 (2012).
- [24] J. García-Torres, A. Serrà, P. Tierno, X. Alcobé, and E. Vallés, Magnetic propulsion of recyclable catalytic nanocleaners for pollutant degradation., *ACS Appl. Mater. Interfaces* **9**, 23859 (2017).
- [25] K. Keshoju, H. Xing, and L. Suna, Magnetic field driven nanowire rotation in suspension, *Appl. Phys. Lett.* **91**, 123114 (2007).
- [26] L. Chevy, N. K. Sampathkumar, A. Cebers, and J.-F. Berret, Magnetic wire-based sensors for the microrheology of complex fluids, *Phys. Rev. E* **88**, 062306 (2013).
- [27] L. Zhang, T. Petit, Y. Lu, B. E. Kratochvil, K. E. Peyer, R. Pei, J. Lou, and B. J. Nelson, Controlled propulsion and cargo transport of rotating nickel nanowires near a patterned solid surface, *ACS nano* **4**, 6228 (2010).
- [28] P. Tierno and A. Snezhko, Transport and assembly of magnetic surface rotors., *ChemNanoMat* **7**, 881 (2021).
- [29] G. Junot, C. Calero, J. García-Torres, I. Pagonabarraga, and P. Tierno, Unveiling the rolling to kayak transition in propelling nanorods with cargo trapping and pumping, *Nano Letters* **23**, 850 (2023).
- [30] S. H. Lee and C. M. Liddell, Anisotropic magnetic colloids: A strategy to form complexstructures using non-spherical building blocks, *Small* **571**, 1957 (2009).
- [31] J. Palacci, S. Sacanna, A. P. Steinberg, D. J. Pine, and P. M. Chaikin, Living crystals of light-activated colloidal surfers, *Science* **339**, 936 (2013).
- [32] F. Martinez-Pedrero, H. Massana-Cid, and P. Tierno, Assembly and transport of microscopic cargos via reconfigurable photoactivated magnetic microdockers, *Small* **13**, 1603449 (2017).
- [33] J. Palacci, S. Sacanna, A. Vatchinsky, P. M. Chaikin, and D. J. Pine, Photoactivated colloidal dockers for cargo transportation, *J. Am. Chem. Soc.* **135**, 15978 (2013).
- [34] F. Martinez-Pedrero, A. Cebers, and P. Tierno, Orientational dynamics of colloidal ribbons self-assembled from microscopic magnetic ellipsoids, *Soft Matter* **12**, 3688 (2016).
- [35] J. Happel and H. Brenner, *Low Reynolds number hydrodynamics* (Springer, Dordrecht, Netherlands, 1983).
- [36] P. Lenz, J.-F. m. c. Joanny, F. Jülicher, and J. Prost, Membranes with rotating motors, *Phys. Rev. Lett.* **91**, 108104 (2003).
- [37] J. Simmchen, J. Katuri, W. E. Uspal, M. N. Popescu, M. Tasinkevych, and S. Sánchez, Topographical path-

- ways guide chemical microswimmers, *Nat. Commun.* **7**, 10598 (2016).
- [38] W. E. Uspal, M. N. Popescu, S. Dietrich, and M. Tasinkevych, Guiding catalytically active particles with chemically patterned surfaces, *Phys. Rev. Lett.* **117**, 048002 (2016).
- [39] S. Ketzetzi, J. de Graaf, R. P. Doherty, and D. J. Kraft, Slip length dependent propulsion speed of catalytic colloidal swimmers near walls, *Phys. Rev. Lett.* **124**, 048002 (2020).
- [40] D. Boniface, S. G. Leyva, I. Pagonabarraga, and P. Tierno, Clustering induces switching between phoretic and osmotic propulsion in active colloidal rafts, *Nat. Commun.* **1**, 5666 (2024).
- [41] H. Massana-Cid, J. Codina, I. Pagonabarraga, and P. Tierno, Active apolar doping determines routes to colloidal clusters and gels, *Proc. Natl. Acad. Sci. USA* **115**, 10618 (2018).
- [42] A. Terray, J. Oakey, and D. W. M. Marr, Microfluidic control using colloidal devices, *Science* **296**, 1841 (2002).
- [43] P. Tierno, R. Golestanian, I. Pagonabarraga, and F. Sagués, Magnetically actuated colloidal microswimmers, *J. Phys. Chem. B* **112**, 16525 (2008).